




Neuronal hypertrophy dampens neuronal intrinsic excitability and stress responsiveness during chronic stress

Sara Matovic^{1,2}, Aoi Ichiyama², Hiroyuki Igarashi¹, Eric W. Salter^{1,7}, Julia K. Sunstrum² , Xue Fan Wang³, Mathilde Henry^{4,8}, Eric S. Kuebler¹, Nathalie Vernoux⁴, Julio Martinez-Trujillo^{1,2,3}, Marie-Eve Tremblay^{4,5,6}  and Wataru Inoue^{1,2,3} 

¹Robarts Research Institute, University of Western Ontario

²Neuroscience Program, University of Western Ontario

³Department of Physiology and Pharmacology, Schulich School of Medicine and Dentistry, University of Western Ontario

⁴Axe Neurosciences, CRCHU de Quebec-Université Laval

⁵Département de médecine moléculaire, Université Laval

⁶Division of Medical Sciences, University of Victoria

⁷Current address: University of Toronto

⁸Current address: INRAE, Univ. Bordeaux, Bordeaux INP, Nutrineuro, UMR 1286, Bordeaux, F-33000, France

Edited by: Ole Paulsen & Yasuhiko Minokoshi

Linked articles: This article is highlighted in a Perspectives article by Onaka. To read this article, visit <https://doi.org/10.1113/JP280033>.

Key points

- The hypothalamic-pituitary-adrenal (HPA) axis habituates to repeated stress exposure.
- We studied hypothalamic corticotropin-releasing hormone (CRH) neurons that form the apex of the HPA axis in a mouse model of stress habituation using repeated restraint.
- The intrinsic excitability of CRH neurons decreased after repeated stress in a time course that coincided with the development of HPA axis habituation.
- This intrinsic excitability plasticity co-developed with an expansion of surface membrane area, which increased a passive electric load and dampened membrane depolarization in response to the influx of positive charge.
- We report a novel structure–function relationship for intrinsic excitability plasticity as a neural correlate for HPA axis habituation.

Abstract Encountering a stressor immediately activates the hypothalamic-pituitary-adrenal (HPA) axis, but this stereotypic stress response also undergoes experience-dependent adaptation. Despite the biological and clinical importance, how the brain adjusts stress responsiveness in the long term remains poorly understood. We studied hypothalamic corticotropin-releasing hormone neurons that form the apex of the HPA axis in a mouse model of stress habituation using repeated restraint. Using patch-clamp electrophysiology in acute slices, we found that the intrinsic

Sara Matovic first joined Dr Wataru Inoue's laboratory in 2014 as an honours thesis student for her BSc in Neuroscience. She continued on to complete her MSc in Neuroscience with Dr Inoue, where she examined how the intrinsic excitability of corticotropin-releasing hormone neurons in the paraventricular nucleus of the hypothalamus adapts with chronic stress. Sara currently pursues her interest in stress neurobiology in the field of clinical psychology.



This article was first published as a preprint. Matovic S, Ichiyama A, Igarashi H, Salter EW, Wang XF, Henry M, Vernoux N, Tremblay ME, Inoue W. 2019. Stress-induced neuronal hypertrophy decreases the intrinsic excitability in stress habituation. bioRxiv. <https://doi.org/10.1101/593665>.

excitability of these neurons substantially decreased after daily repeated stress in a time course that coincided with their loss of stress responsiveness *in vivo*. This intrinsic excitability plasticity co-developed with an expansion of surface membrane area, which increased a passive electric load, and dampened membrane depolarization in response to the influx of positive charge. Multiphoton imaging and electron microscopy revealed that repeated stress augmented ruffling of the plasma membrane, suggesting an ultrastructural plasticity that may efficiently accommodate the membrane area expansion. Overall, we report a novel structure–function relationship for intrinsic excitability plasticity as a neural correlate for adaptation of the neuroendocrine stress response.

(Received 11 March 2020; accepted after revision 17 April 2020; first published online 29 April 2020)

Corresponding author W. Inoue: Robarts Research Institute, University of Western Ontario.

Email: winoue@robarts.ca

Introduction

Corticotropin-releasing hormone (CRH) neurons in the paraventricular nucleus of the hypothalamus (PVN) play a key role in the stress response by driving the hypothalamic-pituitary-adrenal (HPA) axis and complex stress-related behaviours (Joëls & Baram, 2009; Bains *et al.* 2015; Füzesi *et al.* 2016; Herman & Tasker, 2016; Sterley *et al.* 2018; Kim *et al.* 2019; Wang *et al.* 2019; Yuan *et al.* 2019). Recent Ca^{2+} imaging studies in freely moving mice revealed that the population activity of PVN-CRH neurons rapidly increases upon exposure to aversive stimuli, and conversely, decreases with rewarding stimuli (Kim *et al.* 2019; Yuan *et al.* 2019), indicating that these neurons bidirectionally encode real-time changes in competing environmental stimuli. While this immediate activation is critical for driving stereotypical responses to imminent threats, the responsiveness of PVN-CRH neurons to environmental stimuli must also be labile and shaped through a prior history of stress to promote long-term adaptation. For example, in both humans and experimental animals, the HPA axis normally habituates to repeated encounters of psychological stress (Aguilera, 1994; Chen & Herbert, 1995; Kirschbaum *et al.* 1995; Bhatnagar *et al.* 2002a; Kim & Han, 2006; Uchida *et al.* 2008). By contrast, a lack of habituation is associated with stress vulnerability and contributes to the maladaptive consequences of chronic stress (McEwen & Seeman, 1999; Epel *et al.* 2000; Kudielka *et al.* 2006; Uchida *et al.* 2008; Gianferante *et al.* 2014). Despite the biological and clinical importance of HPA axis habituation, how PVN-CRH neurons alter their responsiveness to mediate habituation during chronic stress exposure remains largely unknown.

Current descriptions of the neural mechanisms regulating the plasticity of PVN-CRH neurons has focused on the afferent synapses converging from stress-relevant brain areas distributed across the brain (Bains *et al.* 2015; Herman & Tasker, 2016). Diverse types of stressor have been shown to induce functional and structural plasticity of both glutamatergic and GABAergic synapses (Verkuyl *et al.* 2004; Flak *et al.* 2009; Korosi *et al.* 2010; Kuzmiski *et al.* 2010; Miklós & Kovács, 2012; Gunn *et al.* 2013; Inoue *et al.* 2013; Kusek *et al.* 2013; Wamsteeker Cusulin *et al.*

2013a; Salter *et al.* 2018). The resulting changes in the excitation and inhibition balance have been proposed to be important for modulating the activity of PVN-CRH neurons (Verkuyl *et al.* 2004; Korosi *et al.* 2010; Gunn *et al.* 2013). However, synaptic modulation is not the only mode of memory storage, and ample data show that persistent modulation of intrinsic excitability (intrinsic plasticity) also make critical contributions to the cellular process of learning (Daoudal & Debanne, 2003; Zhang & Linden, 2003; Schulz, 2006; Kourrich *et al.* 2015; Debanne *et al.* 2018; Lisman *et al.* 2018). Surprisingly, the intrinsic plasticity of PVN-CRH neurons has not been studied in the context of long-term changes of the HPA axis.

Repeated restraint stress in rodents has been extensively used to study the neuroendocrine habituation that develops slowly, after days and weeks of repeated stress exposure (Kiss & Aguilera, 1993; Ma *et al.* 1999; Stamp & Herbert, 1999; Cole *et al.* 2000; Bhatnagar *et al.* 2002a; Carter *et al.* 2004; Girotti *et al.* 2006). This paradigm offers a simple model to study the plasticity mechanisms that control long-term changes in PVN-CRH neurons' stress sensitivity. Here, we report that the intrinsic excitability of PVN-CRH neurons is strongly attenuated over 21 days of daily repeated restraint in mice, in a time course that coincides with their loss of stress responsiveness *in vivo*. Our data collectively indicate that the decrease in PVN-CRH neurons' intrinsic excitability is due to an increase in the surface membrane area of the soma (i.e. cell size) as a result of increased membrane ruffling. The surface area increase consequently decreases the input (whole-cell) resistance with little change in the specific membrane resistance. Our findings identify a new structure–function relationship involved in intrinsic excitability plasticity as well as a neuronal correlate for HPA axis habituation.

Materials and methods

Animals

All experimental procedures were approved by the University of Western Ontario Animal Use Subcommittee and University Council on Animal Care (AUP: 2018–130)

in accordance with the Canadian Council on Animal Care guidelines. Homozygous *crh-IRES-Cre* (Stock No: 012704, the Jackson Laboratory) and *Ai14* (Stock No: 007908, the Jackson Laboratory) mice were mated, and the resulting heterozygous *crh-IRES-Cre;Ai14* offspring were used as CRH-reporter mice as previously characterized in detail (Wamsteeker Cusulin *et al.* 2013b; Itoi *et al.* 2014; Chen *et al.* 2015). The bright tdTomato expression allows for visual identification of CRH neurons in brain slices prepared for immunohistochemistry, *ex vivo* electrophysiology recordings and multiphoton live slice imaging. PVN-CRH neurons identified in our study do not differentiate between neuroendocrine neurons projecting to the median eminence and preautonomic neurons projecting to the brainstem and spinal cord. All animals used were male and between 8 and 12 weeks of age at the time they were killed. They were group housed (2–4 mice per cage) in a standard shoebox mouse cage supplied with mouse housing, paper nesting materials and wood-chip bedding. The mice were housed on a 12/12 h light/dark cycle (lights on at 07:00) in a temperature-controlled ($23 \pm 1^\circ\text{C}$) room with free access to food and water. Cages were cleaned every 7 days.

Stress protocols

For restraint stress, mice were individually placed in a restrainer constructed from a 50 ml conical tube with multiple ventilation holes. In order to restrict the forward/backward movement of mice, the inner space length of the restrainer was adjusted by moving a disc wall that forms the head end of the restrainer. For repeated restraint stress, the one-hour restraint stress session was repeated for 7 or 21 consecutive days (between 13:00 and 14:00). For stress recovery, a group of mice was first subjected to 21 days of repeated restraint stress and then left undisturbed in their home cage (2–4 mice/cage) for 7 days. The control mice were kept in their home cage (2–4 mice/cage) in the animal housing facility.

Immunohistochemistry

c-Fos expression was examined immediately after a 1 h-long episode of restraint stress that was given for the first time (Acute), one day after 7 or 21 (1 h-long) episodes of daily repeated restraint (7RRS or 21RRS), or one day after 7 days of a no-stress recovery period following the 21RRS (recovery). As a control, we also studied stress-naïve (control) mice (Fig. 1A). The mice were deeply anaesthetized with sodium pentobarbital (100 mg kg^{-1} , intraperitoneally). A tail-pinch test was performed to ensure the depth of anaesthesia. The mice were then transcardially perfused with ice-cold saline solution (0.9% NaCl) followed by 4% paraformaldehyde

(PFA, Sigma) dissolved in phosphate-buffered saline (PBS, pH 7.4). The brains were removed and fixed in 4% PFA at 4°C overnight. The brains were then coronally sectioned into $50 \mu\text{m}$ thick slices using a vibratome (VT1000S, Leica Biosystems, Concord, ON, Canada). Sections were stored in a cryoprotectant solution (30% glycerol, 30% ethylene glycol, in 20 mM PB) at -20°C until use. Immunohistochemistry was performed on free-floating sections. Sections were rinsed in PBS three times for 5 min each and then incubated in a blocking solution (3% normal donkey serum, 0.3% Triton X-100 and 0.03% NaN_3 in PBS) for 1 h. Slices were then incubated with anti-c-Fos rabbit monoclonal antibody (Cell Signalling Technology, cat: 2250S, 1:1000 dilution in blocking solution) overnight at room temperature. After three washes in PBS, the sections were incubated with Alexa Fluor 647 donkey anti-rabbit IgG (ThermoFisher Scientific, cat: A-31573, 1:500 dilution in blocking solution). After three washes with PBS, the sections were incubated in 4',6-diamidino-2-phenylindole (DAPI, 100 ng ml^{-1} in PBS, Sigma, cat: D9542) for 10 min. After two washes with PBS, the sections were mounted on glass slides and cover-slipped using Fluoromount-G mounting medium (Electron Microscopy Sciences (EMS), cat: 17984-25).

c-Fos immunohistochemistry sections (bilateral \times 2 sections = 4 images/mouse) were imaged and analysed as follows. z-stack images ($0.685 \mu\text{m}$ thick optical sections, 20–23 sections) were obtained with a confocal microscope (Leica SP8, Leica-Microsystems) using a $20\times$ objective (HC PL APO CS2, 0.75 NA, dry, Leica-Microsystems). Experimenters were blinded to treatments prior to image analysis. Each image was reconstructed in 3D and quantified using Imaris (Imaris v7.6.4, Bitplane, AG, Zürich, Switzerland). To estimate the volume positive for tdTomato and c-Fos expression, automatic thresholding was applied and a surface was created for each channel. The same threshold values were then used to create a co-localization channel dual-positive for tdTomato and c-Fos. A third surface was then created for the co-localization channel, determining the volume of the co-localization. The degree of c-Fos expression by tdTomato-positive CRH neurons was derived from co-localization volume divided by tdTomato volume for individual images.

Electrophysiology

For the electrophysiology experiments, mice were killed on the day after the last restraint stress (e.g. for 21RRS, sacrifice was on day 22 without restraint stress). Control mice were killed without any stress, and acute-stress mice were restraint-stressed once and killed immediately after the end of the stress. The mice were deeply anaesthetised with isoflurane and decapitated. Brains were then quickly

removed from the skull and placed in icy slicing solution containing (in mM): 87 NaCl, 2.5 KCl, 25 NaHCO₃, 0.5 CaCl₂, 7 MgCl₂, 1.25 NaH₂PO₄, 25 glucose and 75 sucrose (Osmolarity: 315–320 mOsm), saturated with 95% O₂/5% CO₂. 250 µm thick coronal sections containing the PVN were cut using a vibratome (VT1200 S, Leica). Sections were then placed in ACSF containing (in mM): 126 NaCl, 2.5 KCl, 1.25 NaH₂PO₄, 26 NaHCO₃, 10 glucose, 2.5 CaCl₂ and 1.5 MgCl₂ (Osmolarity: 295–300 mOsm), saturated in 95% O₂/5% CO₂, maintained at 36°C for 30 min, and thereafter kept at room temperature in the same ACSF for the rest of the day.

PVN slices were transferred to a recording chamber superfused with ACSF (flow rate 1–2 ml min⁻¹, 28–32°C). Slices were visualized using an upright microscope (BX51WI, Olympus) equipped with infrared differential

interference contrast and epi-fluorescence optics as well as a digital camera (Rolera-XR, Q-Imaging) or an analogue camera (IR-1000, DAGE-MTI). CRH neurons were identified by their expression of tdTomato. Patch-clamp recording pipettes were pulled from borosilicate glass (Cat#: BF150-86-10, Sutter Instrument) using a Flaming/Brown Micro-pipette Puller (P-1000, Sutter Instrument) to a tip resistance of 3–5 MΩ. Electrodes were filled with an internal solution containing (in mM): 108 K-gluconate, 2 MgCl₂, 8 Na-gluconate, 8 KCl, 1 K₂-ethylene glycol-bis(β-aminoethyl ether)-N,N,N',N'-tetraacetic acid (EGTA), 4 K₂-ATP, 0.3 Na₃-GTP, 10 HEPES was used (Osmolarity: 283–289 mOsm, and pH: 7.2–7.4). The calculated liquid junction potential was –12 mV and was used to correct reported membrane potentials.

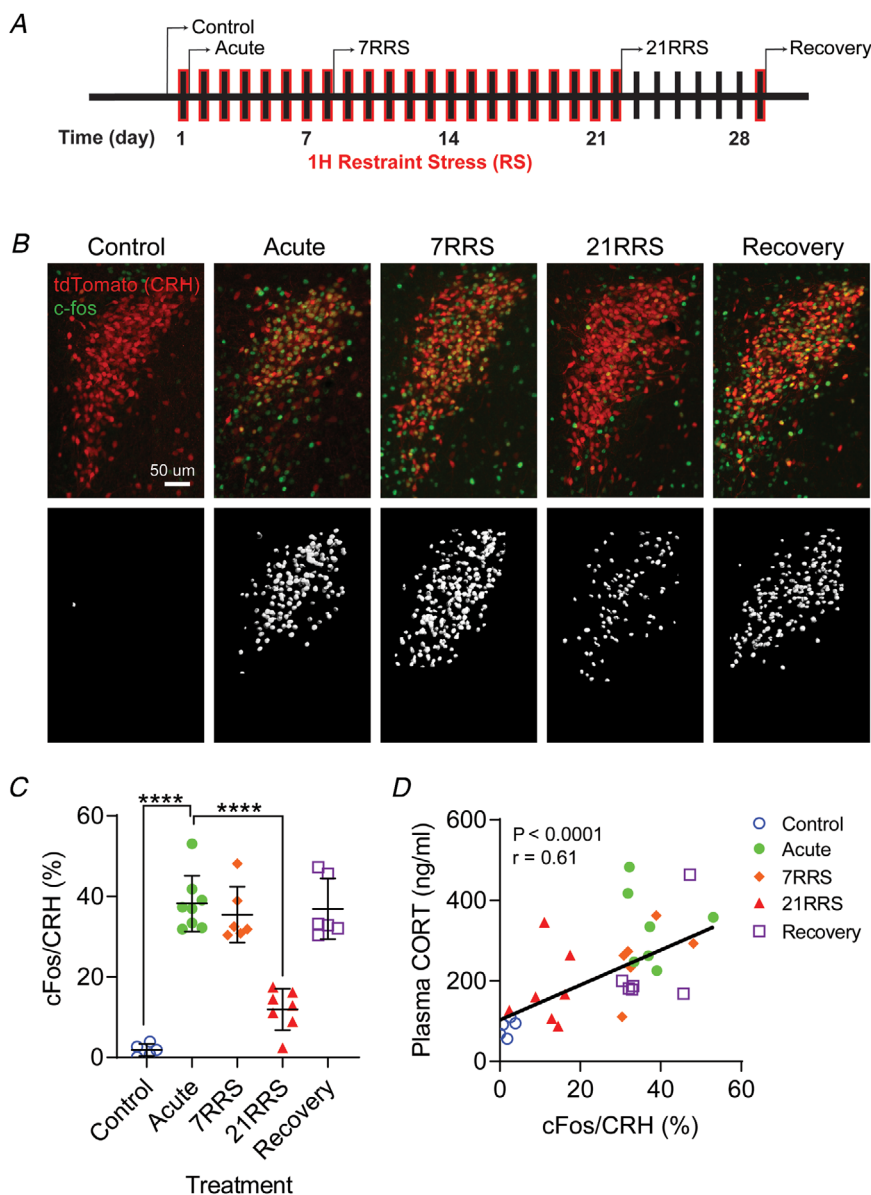


Figure 1. Restraint stress-induced c-Fos expression in PVN-CRH neurons diminishes after repeated stress in a reversible manner

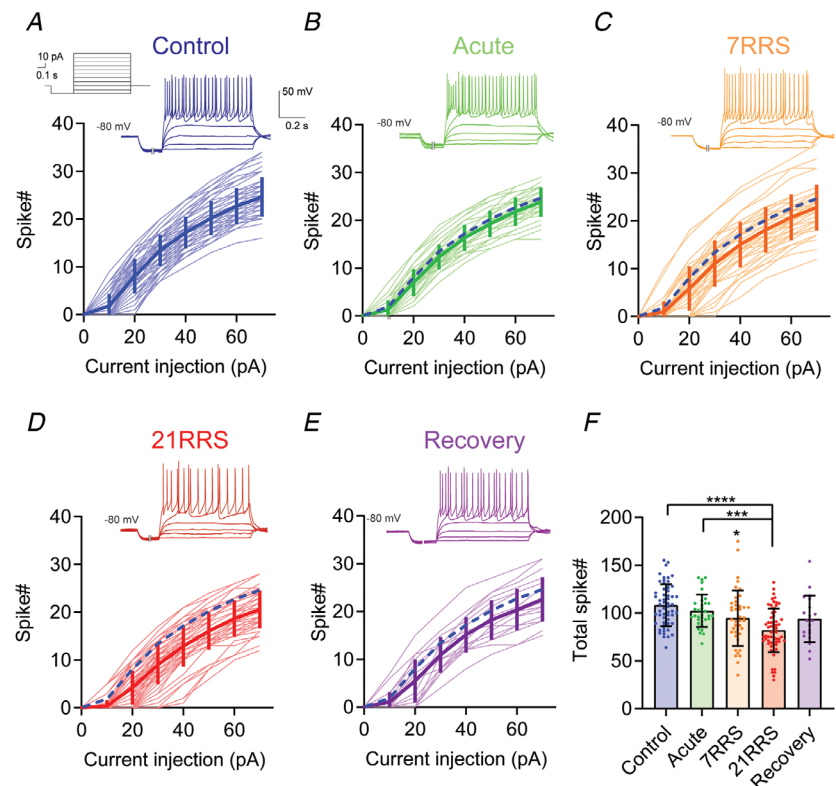
A, experimental timeline. Mice received daily, 1 h-long restraint stress (red) and were perfused immediately after the stress. Control mice were perfused without restraint stress. **B**, top: examples of c-Fos immunohistochemistry (green) and tdTomato expression (red) in the PVN of CRH-tdTomato reporter mice. Bottom: co-localization (white) of c-Fos and tdTomato. **C**, summary graph for c-Fos/tdTomato volume (%). Acute restraint strongly increased c-Fos expression in tdTomato-positive PVN-CRH neurons as compared with control. 21RRS, but not 7RRS, diminished the restraint-induced c-Fos expression. The loss of c-Fos induction spontaneously recovered after a 7-day no-stress recovery period. One-way ANOVA followed by Tukey's multiple comparison test. $F(4, 27) = 44.5$, $P < 0.0001$; **** $P < 0.0001$ for control vs. acute and acute vs. 21RRS. Error bars are SD. **D**, c-Fos expression in PVN-CRH neurons significantly correlated with circulating corticosterone levels. Linear regression, $P < 0.0001$, $r = 0.61$.

Whole-cell patch-clamp recordings were obtained using a Multiclamp 700B amplifier (Molecular Devices), digitized at 10–20 kHz (Digidata 1440, Molecular Devices) and recorded on a PC using pClamp 10 software (Molecular Devices). Input capacitance (C_m) was measured using the Membrane Test protocol implemented in pClamp. Briefly, the electrode capacitance was compensated following gigaseal formation prior to breaking the membrane for establishing the whole-cell configuration. Under whole-cell voltage clamp mode (holding potential at -80 mV), a square wave voltage command (5 mV, 10 ms) was applied. Charge (Q_t) under the transient was calculated as the sum of the area under the curve in the transient above the steady-state current (ΔI) plus a correction factor $\Delta I \cdot \tau$ where τ is a decay time constant of I . $C_m = Q_t / \Delta V$. Signals were low-pass filtered at 10 kHz and averaged 100 times. Recordings were obtained from cells with access resistance below 20 M Ω . The average access resistance was similar between control and 21RRS (control vs. 21RRS: 8.67 ± 3.61 M Ω $n = 72$ vs. 7.58 ± 3.10 M Ω $n = 67$, $P > 0.05$, unpaired t test). Resting membrane potential was measured in $I = 0$ current clamp mode around 2 min after breaking the membrane. To study the input–output relationship, PVN-CRH neurons were depolarized to elicit action potential firing with incremental current injection steps (10 pA for 700 ms) following a brief hyperpolarizing pre-pulse (-20 pA for 300 ms, Fig. 2A). In this experiment, the holding current

($0 - -25$ pA) was adjusted to achieve a membrane potential of -80 mV. ACSF contained kynurenic acid (2 mM, Sigma) and picrotoxin (100 μ M, Sigma) to block ionotropic glutamate and GABA receptors, respectively. For offline analysis of electrophysiological data, Clampfit 10 software (Molecular Devices, San Jose, CA) was used. Resting membrane potential was determined from the peak of the histogram of the data points from an epoch of 10 s gap-free ($I = 0$ mode) recording. The action potential threshold, amplitude, rise slope, and half-width were analysed for the first spike at the rheobase current injection using a custom MATLAB (MathWorks, Natick, MA) algorithm. The slope (dV/dt) was measured by taking the difference in voltage between two time steps and dividing by the resolution of acquisition. The time of the threshold crossing was detected by finding the time point where dV/dt was $\leq 5\%$ of the maximum dV/dt of the rising phase. The amplitude was computed as the difference in voltage between threshold and peak. The rise slope was measured as the maximum dV/dt during the rising phase. The half-width was measured by finding the difference in time between the maximum dV/dt during the rising phase and the strongest negative slope during the falling phase. The following criteria were used to detect repetitive firing of action potentials during current injection steps: 1) the duration from threshold to peak is ≤ 5 ms, 2) amplitude is $\geq 30\%$ of rheobase amplitude, and 3) action potential trough (minimum

Figure 2. Firing frequency of PVN-CRH neurons decreases after repeated stress in a reversible manner

A–E, spike number–current injection curve of individual neurons (thin lines) and the group averages (thick lines) for control (A), acute (B), 7RRS (C) 21RRS (D) and recovery (E) groups. The control average curve is repeatedly shown as a dotted line for comparison purposes. Sample traces recorded from PVN-CRH neurons are shown at the top. Current injection protocol (10 pA increment from -20 pA, holding potential = -80 mV) is shown top-left in (A). Note that traces during the initial hyperpolarization step (0.3 s) are shortened (indicated by two vertical lines) for presentation purposes. F, summary bar graph of total spike number during the current steps, from data shown in A. One-way ANOVA followed by Tukey's multiple comparison test. $F[4, 212] = 10.3$, $P < 0.0001$; **** $P < 0.0001$ for control vs. 21RRS, *** $P = 0.005$ for acute vs. 21RRS, and * $P = 0.037$ for control vs. 7RRS. Error bars are SD. [Colour figure can be viewed at wileyonlinelibrary.com]



membrane potential in the interval between the peaks of two consecutive action potentials) is ≤ -22 mV. In addition, only recordings that elicited equal or greater numbers of action potentials with depolarizing steps of current injections were included in the analysis. The last data inclusion criterion was used to focus on the intrinsic excitability mechanisms that increase firing frequency with increasing current injections, and that receive relatively smaller influences from other mechanisms that diminish action potential firing with progressively larger current injections.

Multiphoton imaging of acute brain slices

Acute PVN slices were imaged using a multiphoton microscope (Bergamo II, Thorlabs Imaging Systems, Sterling, VA) with a 20 \times objective lens (XLUMPLFLN, 1.0 NA, water immersion, Olympus, Tokyo, Japan). The images were acquired with the following settings: 16-bit dynamic range, 6 \times cumulative image averaging, 0.32 \times 0.32 μ m pixel size, 100 μ m z-stack with 0.7 μ m z-axis interval. 1000 nm laser (Chameleon, Coherent Laser Group, Santa Clara, CA) was applied, and the emission signals were detected through a 562 nm edge epi-fluorescence dichroic mirror (FF562-Di03-32 \times 44-FX, Semrock, Rochester, NY) and a 607/70 nm single-band bandpass filter (FF01-607/700-32, Semrock). Multiphoton imaging during electrophysiology recordings was performed with the same multiphoton microscope and objective. Recorded cells were visualized by including Alexa Fluor 488 hydrazide (0.2 mM, ThermoFisher Scientific) in the internal solution. The same optical imaging setup was used and the targeted cells were continuously imaged with 50 μ m z-stack excited at 750 nm and emission signals detected through 562 nm edge epi-fluorescence dichroic mirror and 525/50 nm single-band bandpass filter (FF03-525/50-25, Semrock): 2 \times cumulative averaging at 7.7 fps with 30 s intervals, repeated until the fluorescence disappeared by rupturing. The z-stack images were 3D-reconstructed using Imaris software (Bitplane, Zürich, Switzerland) and the cell soma surface membrane area was calculated by applying automatic thresholds. To measure the cell soma size, a cubic region of interest was applied to encompass only the soma. Experimenters were blinded to treatments prior to image analysis.

Reconstruction of biocytin-filled neurons

To study dendrite branching, biocytin (0.5 % w/v, ThermoFisher Scientific) was included in the internal solution. The slices were fixed in 4% PFA for 24 h at 4°C. The filled cells were then visualized by incubating slices with streptavidin-Alexa 488 (1:500, ThermoFisher Scientific) diluted in PBS containing 2%

TritonX-100. Slices were mounted using a mounting medium (Fluoromount-G, Electron Microscopy Sciences, Hatfield, PA). Dye-filled cells were imaged with a multiphoton microscope (Bergamo II, Thorlabs Imaging Systems) using a 20 \times objective lens (XLUMPLFLN, 1.0 NA, water immersion, Olympus). The images were acquired with the following settings: 16-bit dynamic range, 6 \times cumulative image averaging, 0.073 μ m pixel size, 0.5 μ m z-axis interval. 940 nm laser (Chameleon, Coherent Laser Group, Santa Clara, CA) was applied, and the emission signals were detected through a 562 nm edge epi-fluorescence dichroic mirror and a 525/50 nm single-band bandpass filter. The manual reconstruction of dendritic structure and Sholl analysis were performed using NeuroLucida 360 software (MBF Bioscience). Experimenters were blinded to treatments prior to image analysis.

Electron microscopy

Mice were anaesthetised with pentobarbital (100 mg kg⁻¹, intraperitoneally) and transcardially perfused with PBS followed by 3.5% acrolein and 4% PFA. 50 μ m-thick coronal sections of the brains were cut using a vibratome (Leica Biosystems) and stored at -20 °C in cryoprotectant until further processing. Brain sections were rinsed in PBS (50 mM, pH 7.4) and then quenched with 0.3% hydrogen peroxide (H₂O₂) for 5 min followed by 0.1% sodium borohydride (NaBH₄) for 30 min. Afterwards, sections were rinsed three times in PBS and incubated for 1 h in blocking buffer (10% goat serum, 3% bovine serum albumin, 0.01% Triton X-100) and then overnight with a primary anti-RFP antibody (1:10,000 dilution, Rockland). The next day, sections were rinsed three times in Tris buffer solution and incubated for 2 h with secondary antibody conjugated to biotin (1:300, Jackson ImmunoResearch Laboratories) and then for 1 h with Vectastain Avidin-Biotin Complex Staining kit (Vector Laboratories). Sections were developed in a Tris buffer solution (0.05 M, pH 7.4) containing 0.05% diaminobenzidine and 0.015% H₂O₂ and then rinsed with PBS.

Brain sections containing the PVN from Bregma -0.58 mm to -0.94 mm were used and processed for electron microscopy (Tremblay *et al.* 2010). Briefly, first, brain sections were incubated for 1 h at room temperature in 4% osmium tetroxide (EMS) combined to 3% potassium ferrocyanide in 0.1 M PB. After washing with ddH₂O, brain sections were incubated in a 1% thiocarbohydrazide solution (in ddH₂O) for 20 min at room temperature. A second incubation in 2% osmium tetroxide (in ddH₂O) was next performed for 30 min at room temperature. After washing, sections were dehydrated in increasing concentrations of ethanol, treated with 100% propylene oxide, and impregnated in

Durcupan ACM resin (EMS). Finally, the tissue sections were mounted between ACLAR sheets (EMS), embedded in a thin layer of resin, and placed in a 55°C oven for 3 days of polymerization.

The areas of interest containing the PVN were cut at 70 nm with an ultramicrotome (Leica Ultracut UC7, Leica Biosystems). Ultrathin sections were collected on square-mesh grids and examined at 80 kV using a FEI Tecnai Spirit G2 transmission electron microscope. For analysis, RFP-positive neurons were randomly photographed in each mouse at the sequential magnifications of 900 \times , 1900 \times , and 4800 \times using an ORCA-HR camera (10 MP; Hamamatsu). Membrane contours of RFP-positive neuronal cell bodies ($n = 7$ –10 neurons in each of four control mice and four RRS mice) were drawn using the freehand selection tool of ImageJ 1.6 software. The area and perimeter, as well as the following shape descriptors were determined as detailed elsewhere (Zdilla *et al.* 2016). Circularity = $4\pi \times [\text{Area}]/[\text{Perimeter}]$, solidity $[\text{Area}]/[\text{Convex area}]$, aspect ratio = $[\text{Major axis}]/[\text{Minor axis}]$, and roundness = $4 \times [\text{Area}]/(\pi \times [\text{Major axis}]^2)$.

Statistics

All statistical analyses were performed using GraphPad Prism 8 (Graphpad Software Inc., San Diego, CA). For c-Fos immunohistochemistry, two to four images of the PVN were obtained per animal, and the average value for an individual animal was considered as an N of 1. For electrophysiology, reconstruction of biocytin-filled neurons, electron microscopy and multiphoton imaging data, an individual cell/recording was considered as an n of 1 for the statistical analysis. The number of animals in a treatment group is shown as N. To perform a two-group comparison, an unpaired *t* test and Mann–Whitney test were used for data sets for which a Gaussian distribution was assumed and not, respectively. To compare multiple groups, a one-way ANOVA was performed. Two-way ANOVA was used to conduct multiple-factor comparisons. To examine linear correlations, a linear regression analysis was conducted. $P < 0.05$ was considered statistically significant. Mean values \pm standard deviation (SD) were reported in the text.

Results

PVN-CRH neurons habituate to repeated stress

Exposure to a single restraint stress strongly activates the HPA axis, but this stereotypic neuroendocrine response diminishes after repeated exposures to the same stressor (Kiss & Aguilera, 1993; Bhatnagar *et al.* 2002*b*). This indicates that the HPA axis habituates to repeated restraint

(Grissom & Bhatnagar, 2009) and offers a model to study neural plasticity mechanisms that contribute to the decrease of stress responsiveness. We first characterized the time course of neuronal habituation in mice by studying the loss of PVN-CRH neurons' activity in response to repeated restraint. Using immunohistochemistry, we measured the expression of c-Fos, a marker of recent neuronal activity (Hoffman *et al.* 1993; Kovács, 1998; Girotti *et al.* 2006), in a reporter line in which the fluorescent reporter tdTomato was specifically expressed in the CRH neurons of the PVN (Wamsteeker Cusulin *et al.* 2013*b*; Chen *et al.* 2015). c-Fos expression was examined immediately after a 1 h-long episode of restraint stress that was given for the first time (acute), one day after 7 or 21 (1 h-long) episodes of daily repeated restraint (7RRS or 21RRS), or one day after a 7-day no-stress recovery period following 21RRS (recovery). As a control, we also studied stress-naïve (control) mice (Fig. 1A). As expected, acute restraint strongly increased c-Fos expression in PVN-CRH neurons as compared with controls (one-way ANOVA, Tukey's *post hoc* test; **** $P < 0.0001$, Fig. 1B and C). While 7RRS was not sufficient to decrease the restraint-induced c-Fos expression ($P > 0.99$ vs. acute), 21RRS significantly decreased the c-Fos induction (**** $P < 0.0001$ vs. acute). The loss of restraint-induced c-Fos expression by 21RRS was also reversed after the 7-day no-stress period to a level similar to acute restraint ($P > 0.99$ vs. acute). These results demonstrate that 21RRS, but not 7RRS, decreases the responsiveness of PVN-CRH neurons to the repeated stressor, and that this phenomenon is reversible. We then measured plasma corticosterone levels in the same groups of mice and found a significant positive correlation between the magnitude of c-Fos expression in PVN-CRH neurons and the circulating corticosterone levels (linear correlation, $r = 0.61$, $P < 0.0001$, Fig. 1D). These results suggest that the loss of stress responsiveness in PVN-CRH neurons is a neural correlate for HPA axis habituation to repeated restraint.

Repeated restraint stress decreases the intrinsic excitability of PVN-CRH neurons

Because intrinsic excitability directly influences firing activity, one simple explanation for the loss of c-Fos induction would be a decrease in the intrinsic excitability of PVN-CRH neurons. To test this hypothesis, we conducted whole-cell patch-clamp recordings from PVN-CRH neurons by preparing brain slices one day after 7RRS, 21RRS or (7-day no-stress) recovery period without subjecting the mice to another restraint on the day they were killed (i.e. 24 h after the 7th or 21st restraint). This time point was chosen to study the excitability of PVN-CRH neurons *ex vivo*, with relevance to a lasting change in their responsiveness to restraint *in*

in vivo that was evident 24 h after the 21st restraint. As a control, we also recorded from age-matched, stress-naïve mice as well as immediately after an acute restraint. In the current clamp configuration, PVN-CRH neurons were depolarized to elicit action potential firing with incremental current injection steps ($\Delta = 10$ pA, 700 ms duration) following a brief hyperpolarizing pre-pulse (-20 pA, 300 ms duration, Fig. 2A), a protocol commonly used to characterize PVN neurons (Tasker & Dudek, 1991; Luther *et al.* 2002; Senst *et al.* 2016). In support of our prediction, the intrinsic excitability of PVN-CRH neurons decreased after 3 weeks of RRS, and spontaneously reversed after the no-stress recovery period. Specifically, a single acute stress had no effect on the input-output (i.e. current injection-firing frequency) relationship in comparison with the control. On the other hand, a small rightward shift became evident after 7RRS and became more prominent after 21RRS. Finally, the 7-day no-stress recovery period following 21RRS resulted in a re-normalization of the intrinsic excitability. Fig. 2F re-plots the total spike number of all current injection steps shown in Fig. 2A–E, demonstrating a gradual decrease in the intrinsic excitability during RRS periods (one-way ANOVA, Tukey's *post hoc* test, **** $P < 0.0001$ for 21RRS vs. control) and its spontaneous recovery after the no-stress period ($P = 0.089$ vs. control). These results show that repetitive firing frequency decreases with a time course similar to the habituation of the c-Fos response to restraint stress *in vivo*.

Repeated restraint stress increases cell capacitance (C_m)

We next investigated the cellular mechanisms underlying the stress-induced decrease of intrinsic excitability. To probe potential changes in membrane properties involved in action potential generation, we analysed the kinetics of the first action potentials elicited by the rheobase current injection (the amount of current injection required to trigger the first spike) using the data set shown in Fig. 2. We found no difference in threshold, height, rise slope and half-width of the rheobase action potentials (Table 1). On the other hand, we found that RRS diminished the subthreshold voltage responses to current injection steps (see subthreshold voltage traces shown in Fig. 2A), pointing to changes in the passive membrane properties. Indeed, the input resistance, calculated from the slope of current injection vs. steady-state membrane potential between -10 pA and 0 pA, robustly decreased after 21RRS (one-way ANOVA, Tukey's *post hoc* test; ** $P = 0.0024$ vs. control; Fig. 3A). On the other hand, input resistance did not decrease after acute stress ($P > 0.99$) and 7RRS ($P = 0.12$) as well as after no-stress recovery following 21RRS ($P = 0.24$). These data indicate that input resistance

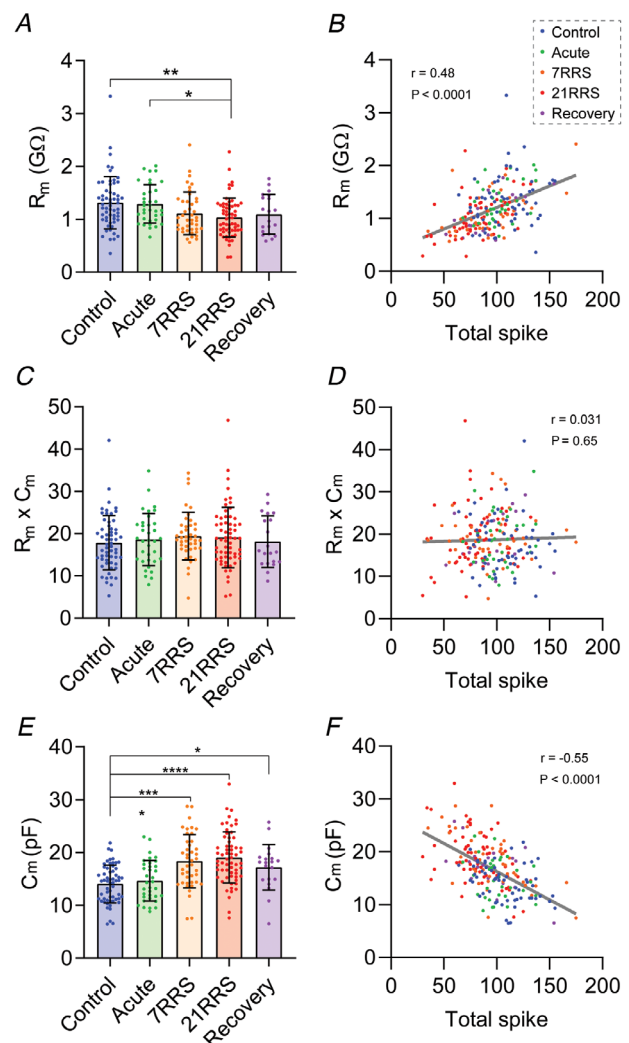


Figure 3. Repeated restraint stress decreases input resistance with complementary increases in C_m

A, summary graphs of the input resistance (R_m). One-way ANOVA followed by Tukey's multiple comparison test. $F [4, 212] = 4.57$, $P = 0.0015$, ** $P = 0.0024$ for control vs. 21RRS, * $P = 0.03$ for acute vs. 21RRS. B, input resistance positively correlated with total spike number elicited during current injection steps. Linear regression. $P < 0.0001$, $r = 0.48$. C, summary graphs of specific membrane resistance normalized by C_m . One-way ANOVA. $F [4, 212] = 0.50$, $P = 0.73$. D, specific resistance did not correlate with total spike number. Linear regression. $P = 0.65$, $r = 0.031$. E, summary graphs of cell capacitance (C_m). One-way ANOVA followed by Tukey's multiple comparison test. $F [4, 212] = 13.3$, $P < 0.0001$, **** $P < 0.0001$ for control vs. 21RRS and acute vs. 21RRS, * $P = 0.045$ for control vs. recovery. F, C_m negatively correlated with total spike number. Linear regression. $P < 0.0001$, $r = -0.55$. Error bars are SD. [Colour figure can be viewed at wileyonlinelibrary.com]

slowly decreases over the course of weeks of RRS and spontaneously reverses with the no-stress period, similar to the firing frequency change. Indeed, the input resistance positively correlated with the total spike number (linear regression, $r = 0.48$, $P < 0.0001$; Fig. 3B), supporting its

Table 1. Properties of rheobase action potential

	Control	Acute	7RRS	21RRS	Recovery	One-way ANOVA F (DFn, DFd)	P value
<i>n</i>	58	35	42	62	20		
Threshold (mV)	-41.0 ± 2.73	-41.3 ± 3.60	-39.7 ± 3.06	-40.4 ± 3.11	-40.0 ± 3.04	F (4, 212) = 1.94	<i>P</i> = 0.10
AP Amp (mV)	66.6 ± 4.96	67.9 ± 5.78	67.8 ± 7.72	67.2 ± 4.49	67.5 ± 4.80	F (4, 212) = 0.49	<i>P</i> = 0.75
AP slope (V/s)	211.0 ± 33.6	229.0 ± 42.6	219.0 ± 43.7	209.0 ± 32.1	219.0 ± 29.3	F (4, 212) = 2.0	<i>P</i> = 0.095
AP half-width (ms)	0.99 ± 0.18	0.97 ± 0.19	0.94 ± 0.17	1.03 ± 0.19	0.95 ± 0.10	F (4, 212) = 1.92	<i>P</i> = 0.11
Rheobase (pA)	15.9 ± 5.6	15.7 ± 5.0	20.2 ± 7.5	21.8 ± 7.6	19.0 ± 7.9	F (4, 212) = 8.05	<i>P</i> < 0.0001

Table 2. Properties at zero current injection

	Control	Acute	7RRS	21RRS	Recovery	One-way ANOVA F (DFn, DFd)	P value
<i>Firing at I = 0 (n)</i>	43	22	26	31	13		
Firing freq (Hz)	4.94 ± 3.0	4.9 ± 3.1	4.35 ± 2.6	3.45 ± 2.3	3.82 ± 3.0	F (4, 130) = 1.63	<i>P</i> = 0.17
<i>Not-firing at I = 0 (n)</i>	15	13	16	31	7		
Vrest (mV)	-69 ± 6.1	-68.6 ± 4.8	-68.3 ± 4.7	-68.9 ± 6.4	-67.4 ± 5.6	F (4, 77) = 0.12	<i>P</i> = 0.97

contribution to the RRS-induced decrease in the intrinsic excitability. In line with the decrease in the input resistance, RRS also increased the rheobase current in a reversible manner (Table 1). Furthermore, at zero current injection, 74% of neurons in control slices spontaneously fired action potentials: the proportion of cells that spontaneously fired had a tendency to decrease after 21RRS (50%), but this change did not reach statistical significance (Chi-square test, *P* = 0.11; Table 2). The frequency of spontaneous firing did not reach significance (one-way ANOVA, *P* = 0.17; Table 2). When resting membrane potentials were analysed from cells that did not spontaneously fire action potentials, we found no difference between groups (one-way ANOVA, *P* > 0.97; Table 2).

Input resistance is the resistance of a whole-cell, which is the product of the specific membrane resistance (i.e. resistance per unit membrane area) and the surface membrane area (i.e. cell size). Intrinsic plasticity commonly involves up- and down-regulation of voltage-gated Na⁺, K⁺, and Ca²⁺ channels (Daoudal & Debanne, 2003; Zhang & Linden, 2003; O'Leary *et al.* 2014; Kourrich *et al.* 2015), which are expected to change the specific membrane resistance. To estimate changes in the specific membrane resistance, we normalized the input resistance by cell capacitance (*C_m*), an electrophysiological measure to estimate surface membrane area (Taylor, 2012) in individual cells. To our surprise, the normalization eliminated the RRS-induced changes (Fig. 3C) and abolished the correlation between the firing frequency and the membrane resistance (*r* = 0.051, *P* = 0.085; Fig. 3D). On the other hand, *C_m* and the input resistance showed a

strong linear negative correlation (*r* = -0.45, *P* < 0.0001), suggesting that the decrease of the input resistance is primarily due to an increase of the surface membrane area. As predicted from these results, *C_m* significantly increased after RRS in a manner that is complementary to the decrease of the input resistance (Fig. 3E). Specifically, acute stress had no effect (one-way ANOVA, Tukey's *post hoc* test, *P* = 0.97 *vs.* control) but 7RRS caused a significant increase in *C_m* (*****P* < 0.0001 *vs.* control). *C_m* remained increased after 21RRS (*****P* < 0.0001 *vs.* control) and partially reversed after the no-stress recovery period (**P* = 0.045 *vs.* control). Moreover, we found a highly significant negative correlation between *C_m* and the total spike number (*r* = -0.53, *P* < 0.0001; Fig. 3F).

Repeated stress increases cell size

Our data so far collectively support a scenario in which PVN-CRH neurons increased their surface membrane area after weeks of RRS, and as a consequence, decreased intrinsic excitability. What are the structural correlates for this plasticity? We first asked if 21RRS increases cell soma size of PVN-CRH neurons, and if so, whether such structural plasticity accounts for the observed increase in *C_m*. With a new cohort of control and 21RRS mice, we prepared acute brain slices and imaged PVN-CRH neurons using two-photon microscopy (Fig. 4A). In the same slices, we subsequently conducted patch-clamp recordings to measure the *C_m* of PVN-CRH neurons. First, the electrophysiological recordings confirmed that 21RRS significantly decreased the firing frequency in this cohort

(control, 98.0 ± 28.8 , $n = 87$ vs. 21RRS, 86.1 ± 25.6 , $n = 104$; $P = 0.003$; unpaired t test) and increased C_m (**** $P < 0.0001$; Fig. 4C); further, total spike number and C_m significantly correlated ($r = -0.57$, $P < 0.0001$). Morphological measurements of these slices found that the surface area of cell soma significantly increased after 21RRS (** $P = 0.0011$, unpaired t test, Fig. 4B).

While the above data support the idea that the hypertrophy of cell soma accounts for the increase in C_m , the magnitude of the structural change (5.4% increase, $516 \pm 68.2 \mu\text{m}^2$ for control vs. $544.0 \pm 73.5 \mu\text{m}^2$ for 21RRS, Fig. 4B) was substantially smaller than that of the C_m change (19.8% increase, 16.7 ± 5.0 pF for control vs. 20.0 ± 5.4 pF for 21RRS, Fig. 4C) measured in the same slices. To identify additional structural correlates for the C_m change, we next examined dendrite morphology by reconstructing the primary branching of a subset of PVN-CRH neurons filled with biocytin after patch-clamp recording (Fig. 4D). In control slices, we found that PVN-CRH neurons have relatively simple morphology, mostly with two to four primary dendrites (control, 2.4 ± 0.5 , $n = 8$) in line with earlier studies in rats (Rho & Swanson, 1989) and mice (Bittar *et al.* 2019). 21RRS did not change the number of primary dendrites (2.9 ± 1.0 , $n = 12$; $P = 0.15$, Mann-Whitney test), total dendrite length (control, $398.4 \pm 89.2 \mu\text{m}$ vs. 21RRS, $401.0 \pm 141.1 \mu\text{m}$, $P = 0.84$, unpaired t test) or the complexity of dendritic branching examined by Sholl analysis (Fig. 4E). These data suggest that changes in dendrite membrane do not explain the RRS-induced C_m increase.

PVN-CRH neurons increase surface membrane complexity after 21RRS

An alternative explanation for the discrepancy between the magnitudes of C_m increase and structural change is that RRS increased the ultrastructural complexities of surface membrane, which contributes to C_m but less to gross cell size observed in light microscopy. This is because the plasma membrane of mammalian cells is not smooth but has many infoldings, ruffles and microvilli (Gentet *et al.* 2000; Pangršič *et al.* 2006). To test this possibility, we flattened out the ruffles and infoldings by artificially expanding the plasma membrane of PVN-CRH neurons, and measured the maximum surface membrane area it could reach before rupture. Specifically, we took advantage of the osmotic drive to expand neurons (Gentet *et al.* 2000; Pangršič *et al.* 2006) by obtaining whole-cell patch-clamp recordings with a high osmolarity (400 mOsm) internal solution with a fluorescent dye (Fig. 5A). We imaged the dye-filled neurons using a multiphoton microscope with simultaneous electrophysiological measurements of C_m . The 'baseline' z-stack image was captured immediately after the start of the whole-cell configuration. The maximum size was measured by the last z-stack imaging before the cell rupture. C_m was recorded intermittently during the imaging period. Fig. 5A shows that dialysis with the high osmolarity internal solution rapidly expanded the soma size and ultimately ruptured the cell. Strikingly, the simultaneous electrophysiological recording did not find any increase in C_m , indicating that the rapid swelling of the soma was not the result of insertion of new

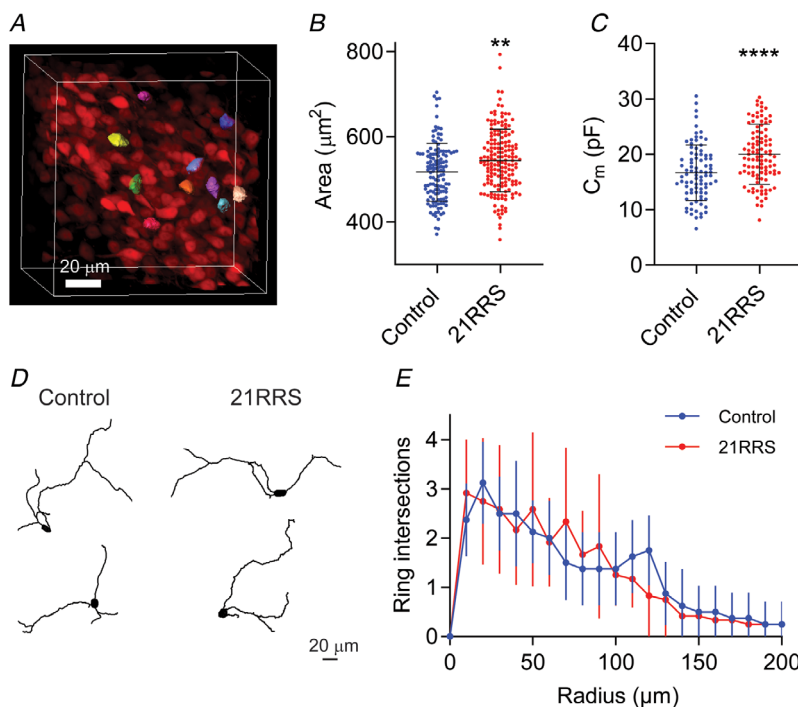


Figure 4. Repeated restraint stress causes hypertrophy of the cell soma with no change in the dendritic complexity

A, a sample image of PVN-CRH neurons in acute brain slices. Examples of the measurement of cell soma surfaces are shown in multiple colours. B, summary graphs of cell soma surface area. Unpaired t test. $P = 0.0011$. Control ($n = 130$), 21RRS ($n = 170$). C, summary graphs of C_m . Unpaired t test. $P < 0.0001$. Control ($n = 87$), 21RRS ($n = 104$). D, samples for the dendrite branching of PVN-CRH neurons. E, summary graph of Sholl analysis. The number of concentric ring intersections did not change after 21RRS. Two-way repeated ANOVA. Interaction, $F [38, 684] = 1.052$, $P = 0.3878$; 21RRS, $F [1, 18] = 0.056$, $P = 0.81$; distance $F [38, 684] = 44.96$, $P < 0.0001$. Error bars are SD.

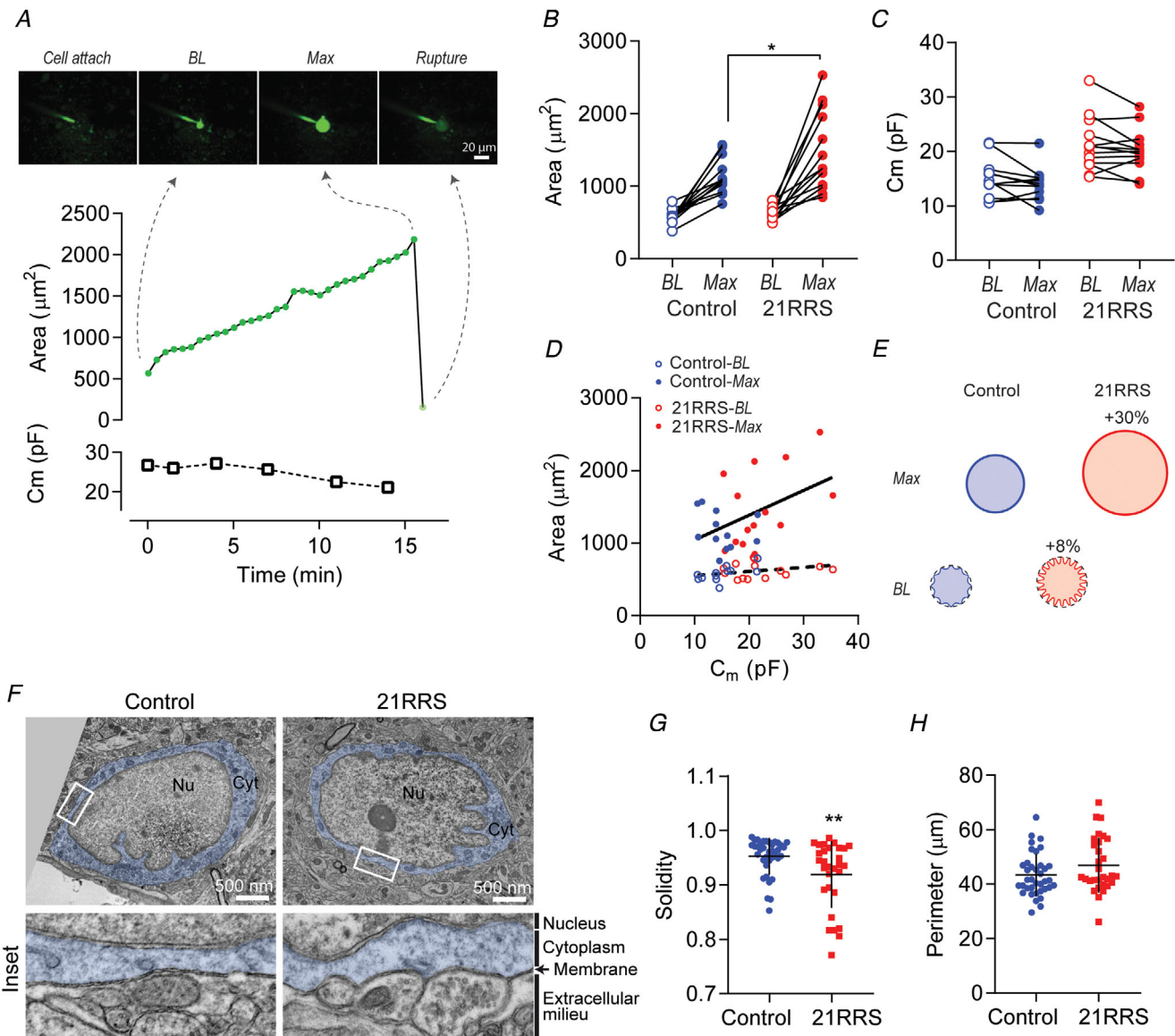


Figure 5. Repeated restraint stress increases surface membrane complexity

A, examples of fluorescent dye-filled PVN-CRH neurons imaged using multiphoton microscopy and simultaneous measurement of C_m . Top: A glass pipette containing a high osmolarity internal solution with Alexa 488 dye attached to the cell (left), immediately after obtaining a whole-cell configuration for the baseline cell soma size measurement (middle-left), the maximum swelling of the cell soma immediately before cell rupture (middle-right), and after cell rupture (right). Bottom: The time course of cell soma surface area and C_m . Note that the abrupt drop of the surface area was due to cell rupture and the loss of fluorescent dye signal. B, summary graph for the cell soma area before and after swelling by high osmolarity internal solution. Two-way repeated measures ANOVA followed by Sidak's multiple comparison test. Interaction $F [1, 23] = 2.80, P = 0.11$, 21RRS $F [1, 23] = 4.45, P = 0.046$. Swelling $F [1, 23] = 64.7, P < 0.0001$. * $P = 0.020$ for control-max vs. 21RRS-max. C, summary graph for C_m before and after swelling by high osmolarity internal solution. Two-way repeated measures ANOVA followed by Sidak's multiple comparison test. Interaction $F [1, 23] = 0.00014, P = 0.99$, 21RRS $F [1, 23] = 17.0, P < 0.0001$. Swelling $F [1, 23] = 4.67, P = 0.041$. D, C_m positively correlated with the soma surface area at maximum swelling (linear regression, $P = 0.02, r = 0.46$) but not at baseline ($P = 0.09, r = 0.34$). E, schematic for our working model. Membrane complexity accommodates RRS-induced surface membrane area (measured at the maximum expansion) with relatively less increase in the gross surface area (measured at the baseline). F, examples of immunohistochemical transmission electron microscopy of the soma of PVN-CRH neurons from control (left) and 21RRS (right) groups. Insets show magnified images of the areas indicated by white rectangles. G, summary graph for solidity of PVN-CRH neurons measured in transmission electron microscopy. Mann-Whitney test ** $P = 0.0092$, control ($n = 37$), 21RRS ($n = 30$). H, summary graph for cell membrane perimeter images. Unpaired t test, $P = 0.1$. Error bars are SD.

membrane and instead likely reflects the flattening of membrane ruffles/irregularities. This is consistent with the ultrastructural complexities of surface membrane reported in various other cell types (Groulx *et al.* 2006; Pangršič *et al.* 2006). The averaged data show that the high osmolarity internal solution dramatically increased the soma surface area in both control and 21RRS (Two-way ANOVA, Sidak's multiple comparison test; $P < 0.0001$ for both control and 21RRS, Fig. 5B), and the soma size in the 21RRS group was significantly larger than controls after swelling ($P = 0.026$, control *vs.* 21RRS, Fig. 5B). By stark contrast, the swelling of the cell did not increase C_m ($P = 0.28$ and 0.24 for control and 21RRS, respectively; Fig. 5C), whereas C_m was significantly larger in 21RRS than the control both at the baseline and after swelling ($P = 0.0006$ for both). Furthermore, C_m significantly correlated with the soma surface area after swelling at the maximum (linear regression, $r = 0.46$, $P = 0.02$), but the correlation was weaker and did not reach statistical significance at the baseline ($r = 0.34$, $P = 0.09$, Fig. 5D). Finally, the RRS-induced increase of the soma surface area was only about 8% at the baseline ($579.3 \pm 101.6 \mu\text{m}^2$ *vs.* $624.7 \pm 106.5 \mu\text{m}^2$ for control *vs.* 21RRS) and about 30% after swelling ($1143.0 \pm 258.5 \mu\text{m}^2$ *vs.* $1484 \pm 553.2 \mu\text{m}^2$ for control *vs.* 21RRS, Fig. 5E). The latter surface area difference was closer to the magnitude of RRS-induced C_m increase, which was 41% measured in the same cells ($15.0 \pm 3.6 \text{ pF}$ *vs.* $21.3 \pm 4.9 \text{ pF}$ for control *vs.* 21RRS). These data support the idea that PVN-CRH neurons have substantial complexities of surface membrane, which contributed to the surface area increase after 21RRS with a relatively smaller increase in the apparent (i.e. without artificial swelling) surface area. Thus, our data offer a solution for the discrepancy between the magnitude of RRS-induced increase in the gross soma size and C_m .

In order to directly examine the ultrastructural complexities of cell membrane at nanoscale resolution, we used immunohistochemical transmission electron microscopy and obtained images of tdTomato-immunopositive neurons in the PVN (i.e. CRH-PVN neurons) of control and 21RRS groups. In line with our electrophysiology and multiphoton imaging data, the plasma membrane delineating the soma of PVN-CRH neurons contain numerous curvatures, and it appeared to be more ruffled after 21RRS *vs.* control (Fig. 5F insets). This observation was supported by our quantitative analysis revealing a significant decrease in the solidity, a measure that describes the extent of concavity in the structure (Zdilla *et al.* 2016), after 21RRS (control *vs.* 21RRS: 0.95 ± 0.034 , $n = 37$ *vs.* 0.92 ± 0.061 , $n = 30$; $P = 0.0092$, Mann-Whitney test; Fig. 5G). Other measures of changes in surface shape, including cross-section area, circularity, roundness and aspect ratio (Zdilla *et al.* 2016), did not reach statistical significance but showed trends that were consistent with an increase in concavity of the soma after 21RRS (Table 3).

Table 3. Ultrastructural properties

	Control 37	21RRS 30	<i>P</i> value
<i>n</i>			
Area (nm ²)	116.2 ± 32.5	122.5 ± 38.5	<i>P</i> = 0.47
Circularity	0.78 ± 0.12	0.71 ± 0.14	<i>P</i> = 0.07
Aspect ratio	1.53 ± 0.56	1.69 ± 0.44	<i>P</i> = 0.12
Roundness	0.67 ± 0.16	0.63 ± 0.16	<i>P</i> = 0.18

In summary, these data indicate that 21RRS increased ultrastructural irregularity of the plasma membrane, which increases the total membrane surface.

Discussion

We show that PVN-CRH neurons, which initiate the neuroendocrine stress response, substantially decrease their intrinsic excitability over the course of daily repeated restraint, in a time course that coincides with their loss of stress responsiveness *in vivo*. Mechanistically, the decrease of intrinsic excitability can be explained by an increase in surface membrane area (i.e. cell size). The direct consequence of cell size increase is a passive electric load, which dampens neurons' voltage responses and firing outputs to the influx of positive charges. Thus, our data demonstrate a novel structure–function relationship underlying the plasticity of intrinsic excitability that manifests as a neural correlate for the habituation of the neuroendocrine stress response.

While synaptic plasticity has been the central focus of the neurobiology of learning and memory, ample data also support the importance of experience-induced plasticity of intrinsic excitability in various neuronal types, species and learning paradigms (Daoudal & Debanne, 2003; Zhang & Linden, 2003; O'Leary *et al.* 2014; Kourrich *et al.* 2015). Here, we report a novel mechanism for intrinsic plasticity, whereby PVN-CRH neurons decreased the input resistance with a parallel increase in C_m (an estimate for surface membrane area) after weeks of daily restraint stress. In principle, a decrease in the input resistance can be attributed to changes in two parameters: 1) an increase in cell surface area and 2) a decrease in the specific membrane resistance. Because normalization of input resistance by C_m abolished the stress-induced change, we propose that repeated restraint stress decreased the input resistance of PVN-CRH neurons primarily by increasing the cell surface area with little change in the specific membrane resistance. Finally, the stress-induced changes in the input resistance and C_m are reversible after one week of no stress, which mirrors the reversal of HPA axis responsiveness. Our data demonstrating plasticity of passive membrane properties are in contrast with the

common forms of intrinsic plasticity described to date, which involve changes in the active membrane properties such as up- and down-regulation of voltage-gated Na⁺, K⁺, and Ca²⁺ channels (Daoudal & Debanne, 2003; Zhang & Linden, 2003; Dong *et al.* 2006; Kourrich & Thomas, 2009; O'Leary *et al.* 2014; Kourrich *et al.* 2015). Changes to active membrane properties can often be probed by changes in action potential threshold and amplitude (Zhang *et al.* 1998; Dong *et al.* 2006; Kourrich & Thomas, 2009). Our study, however, found no change in these action potential properties. In PVN-CRH neurons, it has been reported that a single swim stress rapidly increases firing latency through A-type K⁺ conductance in young (P22–35) mice (Senst *et al.* 2016). Our study, using restraint in adult mice (8–12 weeks old), found a similar but less robust change that did not reach statistical significance and did not further develop after weeks of repeated restraint (data not shown). While our study does not exclude potential changes in the active membrane properties of PVN-CRH neurons after RRS, it sheds light on a previously underappreciated model of plasticity of surface membrane area, which develops after days of repeated stress and controls a passive electronic load to powerfully dampen intrinsic excitability.

The importance of surface membrane area in the control of intrinsic excitability has been elegantly shown in cerebellar Purkinje neurons and cortical pyramidal neurons (Bekkers & Häusser, 2007). By taking advantage of the extensively branched dendrites in these neurons, this study pinched the primary dendrite of a single neuron in brain slices in order to reversibly occlude the dendritic membrane. The occlusion substantially decreased C_m and increased the input resistance, as well as caused a leftward shift in the input–output relationship, demonstrating a direct consequence of membrane area acting as a passive electronic load. Francis *et al.* (2017) recently reported that chronic social defeat stress increases intrinsic excitability of dopamine D1 containing medium spiny neurons in the nucleus accumbens, and that this functional plasticity was accompanied by dendritic atrophy with an increase in the input resistance and a decrease in C_m (Francis *et al.* 2017). On the other hand, hypophyseal neuroendocrine neurons that secrete vasopressin and oxytocin show hypertrophy of neuronal soma in physiological states known to drive their activity, such as dehydration (Marzban *et al.* 1992; Miyata *et al.* 1994) and lactation (Theodosios & Poulain, 1984). It is worth mentioning that, in our model of repeated restraint, plasma osmolarity remains normosmotic after 21RRS (control *vs.* 21RRS; 314.4 ± 3.4 mOsm, *n* = 4 *vs.* 314.5 ± 4.4 mOsm, *n* = 4; unpaired *t* test, *P* = 0.97). Thus, we speculate that multiple homeostatic challenges can drive somatic hypertrophy in hypothalamic neurons. Stimulus specificity and generalizability across different cell types that undergo structural and functional plasticity warrants future investigation. In summary,

in addition to ion channel modulations, changes in surface membrane area, whether they arise from soma or dendrites, are emerging as an important mechanism for experience-induced plasticity of intrinsic excitability.

The C_m we measured in this study was an 'apparent' total cell capacitance that was measured in voltage-clamp by delivering a small subthreshold step near the resting membrane potential of the cells. While this method is widely used, including in the studies discussed above (Bekkers & Häusser, 2007; Francis *et al.* 2017), it does not accurately measure the total capacitance of cells that have complex anatomical structures (e.g. neurons) (Golowasch *et al.* 2009). More specifically, the readout of C_m counts the capacitance of a membrane that is 'well-clamped' and underestimates the parts of the cell that are 'partly-clamped' (Taylor, 2012). Thus, changes in distal dendrites, which may occur during chronic stress, are inherently underestimated. However, the flip side of the coin is that our C_m readouts, which detected stress-induced increases, are indicative of membrane area changes in the soma and proximal dendrites. Consistent with this idea, we found a significant stress-induced increase in the surface area of the soma in acute brain slices. Further, our analysis of biotin-filled neurons found that the branching patterns of dendrites did not change. While the relative contribution of dendritic membrane to our C_m readout remains unknown, we conclude that somatic hypertrophy largely explains the increase in C_m of PVN-CRH neurons.

Our simultaneous multiphoton imaging and patch-clamp electrophysiology showed that the gross cell surface area of PVN-CRH neurons does not fully represent the surface membrane area that biophysically contributes to C_m and input resistance. Several groups have used osmotic manipulation to swell cells and optically measure the cell surface membrane area during patch-clamp recordings in various cell types (Graf *et al.* 1995; Pangršič *et al.* 2006) including hypothalamic and hippocampal neurons (Zhang & Bourque, 2003). Specifically, these studies applied hypoosmotic extracellular medium to isolated cells adhered to a culture dish. The same approach was not feasible with brain slices because the application of hypoosmotic medium caused a massive swelling of the slice tissue, which prevented continuous imaging or patch-clamp recording. Thus, we modified the approach and used a hyperosmotic internal solution (with a fluorescent dye for imaging) while keeping the slices in normoosmotic extracellular medium. This approach rapidly swelled the cell (typically ruptured within 15 min) and allowed for simultaneous multiphoton imaging and whole-cell patch-clamp recording. Importantly, we show that this rapid swelling did not increase C_m, indicating that it occurs by drawing membrane from a pre-existing surface membrane that has already contributed to C_m readouts prior to the osmotic swelling. Therefore, our

data demonstrate that there is a substantial amount of hidden surface membrane as the cell soma surface area expanded to more than twice the baseline both in naïve and 21RRS cells. Similar surface membrane ‘reserves’ have been reported to accommodate a rapid and substantial expansion of surface area in astrocytes (Pangršič *et al.* 2006) and hepatocytes (Graf *et al.* 1995), as well as several cell lines (Groulx *et al.* 2006), suggesting that it is a generalizable mechanism across various cell types.

What is the structural basis for this surface membrane ‘reserve’? The plasma membrane of mammalian cells is not smooth due to various ultrastructural irregularities such as ruffles, infoldings and microvilli, which account for more surface membrane area than the gross size observed at the light and confocal microscopy resolutions (Dai *et al.* 1998; Gentet *et al.* 2000; Groulx *et al.* 2006). Our electron microscopy experiments found that the soma membrane of PVN-CRH neurons have many ruffles, and that there are more ruffles observed after 21RRS than control as indicated by a decrease in solidity. On the other hand, there are few, if any, prominent infoldings or microvilli, which have been reported in non-neuronal cells (Gentet *et al.* 2000), in PVN-CRH neurons in control or 21RRS conditions. While these increased surface irregularities might reflect a process of cell size expansion, it is tempting to speculate that they may also be a biological strategy to accommodate surface membrane area increase with proportionally less expansion of gross cell volume.

Habituation of the HPA axis response to recurrent stressors is a fundamental aspect of stress adaptation observed both in human and experimental animals (Aguilera, 1994; Kirschbaum *et al.* 1995; McEwen & Seeman, 1999; Bhatnagar *et al.* 2002a; Uchida *et al.* 2008). By demonstrating a decrease in the intrinsic excitability of PVN-CRH neurons, which co-develops with the loss of c-Fos induction response to restraint, our findings offer a novel plasticity mechanism that contributes to the neuroendocrine habituation to repeated restraint. Given recent findings that PVN-CRH neurons bidirectionally encode real-time changes in aversive and rewarding stimuli (Kim *et al.* 2019; Yuan *et al.* 2019), and drive behaviour (Füzesi *et al.* 2016), pheromone release (Sterley *et al.* 2018) and encode stress controllability (Daviu *et al.* 2020) independently of the HPA axis, their plasticity of intrinsic excitability likely has versatile roles in stress adaptation. Beyond PVN-CRH neurons, earlier studies using repeated restraint also reported a similar reduction of c-Fos induction in various stress-responsive brain areas, including the amygdala, the prefrontal cortex, the locus coeruleus and the lateral septum (Melia *et al.* 1994; Stamp & Herbert, 1999; Girotti *et al.* 2006; Ons *et al.* 2010). The reduced stress responsiveness of these brain areas, which ultimately send signals to PVN-CRH neurons (Ulrich-Lai & Herman, 2009), would result in decreased stimulus inputs to PVN-CRH neurons. Thus,

the upstream brain mechanisms would work additively with the intrinsic plasticity of the postsynaptic PVN-CRH neurons, diminishing the overall responsiveness of the HPA axis.

In addition to habituation, repeated presentation of a stimulus, including restraint, leads to a response sensitization to a novel stressor (Aguilera, 1994; Bhatnagar & Dallman, 1998). How does the decrease of intrinsic excitability of PVN-CRH neurons accommodate a sensitized response to a novel stressor? In their theory of behavioural habituation, Groves & Thomson have postulated two neural processes, one decremental (habituation) and one incremental (sensitization) that work independently and interact to yield a final behavioural outcome (Groves & Thompson, 1970). Thus, one possibility would be that a novel stressor generates a greater, sensitized input stimulus to PVN-CRH neurons. In this regard, plasticity of passive electronic load is well suited to shift the input–output relationship to produce habituation, while a sensitized excitatory drive can produce greater than normal firing activity. Along the same line, Herman and colleagues reported a similar somatic hypertrophy of immunohistochemically identified PVN-CRH neurons using confocal microscopy after chronic variable stress in rats (Flak *et al.* 2009). Unlike repeated restraint, however, chronic variable stress does not result in habituation but instead causes sensitization of the HPA axis (Miklós & Kovács, 2012; Franco *et al.* 2016). Future studies are warranted to understand how chronic variable stress overcomes the decreased excitability of PVN-CRH neurons predicted from somatic hypertrophy. One possibility is synaptic plasticity that increases excitatory inputs to PVN-CRH neurons, as reported by multiple studies (Verkuyl *et al.* 2004; Flak *et al.* 2009; Miklós & Kovács, 2012; Franco *et al.* 2016; Salter *et al.* 2018).

In summary, we have demonstrated that PVN-CRH neurons substantially decrease their intrinsic excitability over the course of daily repeated restraint, with a time course that coincides with their loss of stress responsiveness *in vivo*. This decrease of intrinsic excitability is best explained by an increase in the surface membrane area and structural plasticity of PVN-CRH neurons. Taken together, we report a novel structure–function relationship for the plasticity of intrinsic excitability that co-develops with the habituation of the neuroendocrine response to repeated stress.

References

- Aguilera G (1994). Regulation of pituitary ACTH secretion during chronic stress. *Front Neuroendocrinol* **15**, 321–350.
- Bains JS, Cusulin JIW & Inoue W (2015). Stress-related synaptic plasticity in the hypothalamus. *Nat Rev Neurosci* **16**, 377–388.

- Bekkers JM & Häusser M (2007). Targeted dendrotomy reveals active and passive contributions of the dendritic tree to synaptic integration and neuronal output. *Proc Natl Acad Sci U S A* **104**, 11447–11452.
- Bhatnagar S & Dallman M (1998). Neuroanatomical basis for facilitation of hypothalamic-pituitary-adrenal responses to a novel stressor after chronic stress. *Neuroscience* **84**, 1025–1039.
- Bhatnagar S, Huber R, Nowak N & Trotter P (2002a). Lesions of the posterior paraventricular thalamus block habituation of hypothalamic-pituitary-adrenal responses to repeated restraint. *J Neuroendocrinol* **14**, 403–410.
- Bhatnagar S, Huber R, Nowak N & Trotter P (2002b). Lesions of the Posterior Paraventricular Thalamus Block Habituation of Hypothalamic-Pituitary-Adrenal Responses to Repeated Restraint. *J Neuroendocrinol* **14**, 403–410.
- Bittar TP, Nair BB, Kim JS, Chandrasekera D, Sherrington A & Iremonger KJ (2019). Corticosterone mediated functional and structural plasticity in corticotropin-releasing hormone neurons. *Neuropharmacology*; <https://doi.org/10.1016/j.neuropharm.2019.02.017>.
- Carter RN, Pinnock SB & Herbert J (2004). Does the amygdala modulate adaptation to repeated stress? *Neuroscience* **126**, 9–19.
- Chen X & Herbert J (1995). Regional changes in c-fos expression in the basal forebrain and brainstem during adaptation to repeated stress: Correlations with cardiovascular, hypothermic and endocrine responses. *Neuroscience* **64**, 675–685.
- Chen Y, Molet J, Gunn BG, Ressler K & Baram TZ (2015). Diversity of Reporter Expression Patterns in Transgenic Mouse Lines Targeting Corticotropin-Releasing Hormone-Expressing Neurons. *Endocrinology* **156**, 4769–4780.
- Cole MA, Kalman BA, Pace TW, Topczewski F, Lowrey MJ & Spencer RL (2000). Selective blockade of the mineralocorticoid receptor impairs hypothalamic-pituitary-adrenal axis expression of habituation. *J Neuroendocrinol* **12**, 1034–1042.
- Dai J, Sheetz MP, Wan X & Morris CE (1998). Membrane Tension in Swelling and Shrinking Molluscan Neurons. *J Neurosci* **18**, 6681–6692.
- Daoudal G & Debanne D (2003). Long-term plasticity of intrinsic excitability: learning rules and mechanisms. *Learn Mem Cold Spring Harb N* **10**, 456–465.
- Daviu N, Füzesi T, Rosenegger DG, Rasiah NP, Sterley T-L, Peringod G & Bains JS (2020). Paraventricular nucleus CRH neurons encode stress controllability and regulate defensive behavior selection. *Nat Neurosci*; DOI: 10.1038/s41593-020-0591-0.
- Debanne D, Inglebert Y & Russier M (2018). Plasticity of intrinsic neuronal excitability. *Curr Opin Neurobiol* **54**, 73–82.
- Dong Y, Green T, Saal D, Marie H, Neve R, Nestler EJ & Malenka RC (2006). CREB modulates excitability of nucleus accumbens neurons. *Nat Neurosci* **9**, 475–477.
- Epel ES, McEwen B, Seeman T, Matthews K, Castellazzo G, Brownell KD, Bell J & Ickovics JR (2000). Stress and body shape: stress-induced cortisol secretion is consistently greater among women with central fat. *Psychosom Med* **62**, 623–632.
- Flak JN, Ostrander MM, Tasker JG & Herman JP (2009). Chronic stress-induced neurotransmitter plasticity in the PVN. *J Comp Neurol* **517**, 156–165.
- Francis TC, Chandra R, Gaynor A, Konkalmatt P, Metzbower SR, Evans B, Engeln M, Blanpied TA & Lobo MK (2017). Molecular basis of dendritic atrophy and activity in stress susceptibility. *Mol Psychiatry* **22**, 1512–1519.
- Franco AJ, Chen C, Scullen T, Zsombok A, Salahudeen AA, Di S, Herman JP & Tasker JG (2016). Sensitization of the Hypothalamic-Pituitary-Adrenal Axis in a Male Rat Chronic Stress Model. *Endocrinology* **157**, 2346–2355.
- Füzesi T, Daviu N, Wamsteeker Cusulin JI, Bonin RP & Bains JS (2016). Hypothalamic CRH neurons orchestrate complex behaviours after stress. *Nat Commun* **7**, 11937.
- Gettet LJ, Stuart GJ & Clements JD (2000). Direct Measurement of Specific Membrane Capacitance in Neurons. *Biophys J* **79**, 314–320.
- Gianferante D, Thoma MV, Hanlin L, Chen X, Breines JG, Zoccola PM & Rohleder N (2014). Post-stress rumination predicts HPA axis responses to repeated acute stress. *Psychoneuroendocrinology* **49**, 244–252.
- Girotti M, Pace TWW, Gaylord RI, Rubin BA, Herman JP & Spencer RL (2006). Habituation to repeated restraint stress is associated with lack of stress-induced c-fos expression in primary sensory processing areas of the rat brain. *Neuroscience* **138**, 1067–1081.
- Golowasch J, Thomas G, Taylor AL, Patel A, Pineda A, Khalil C & Nadim F (2009). Membrane capacitance measurements revisited: dependence of capacitance value on measurement method in nonisopotential neurons. *J Neurophysiol* **102**, 2161–2175.
- Graf J, Rupnik M, Zupancic G & Zorec R (1995). Osmotic swelling of hepatocytes increases membrane conductance but not membrane capacitance. *Biophys J* **68**, 1359–1363.
- Grissom N & Bhatnagar S (2009). Habituation to repeated stress: get used to it. *Neurobiol Learn Mem* **92**, 215–224.
- Groulx N, Boudreault F, Orlov SN & Grygorczyk R (2006). Membrane reserves and hypotonic cell swelling. *J Membr Biol* **214**, 43–56.
- Groves PM & Thompson RF (1970). Habituation: A dual-process theory. *Psychol Rev* **77**, 419–450.
- Gunn BG, Cunningham L, Cooper MA, Corteen NL, Seifi M, Swinny JD, Lambert JJ & Beelli D (2013). Dysfunctional astrocytic and synaptic regulation of hypothalamic glutamatergic transmission in a mouse model of early-life adversity: relevance to neurosteroids and programming of the stress response. *J Neurosci Off J Soc Neurosci* **33**, 19534–19554.
- Herman JP & Tasker JG (2016). Paraventricular Hypothalamic Mechanisms of Chronic Stress Adaptation. *Front Endocrinol* **7**, 137.
- Hoffman GE, Smith MS & Verbalis JG (1993). c-Fos and Related Immediate Early Gene Products as Markers of Activity in Neuroendocrine Systems. *Front Neuroendocrinol* **14**, 173–213.
- Inoue W, Baimoukhametova DV, Füzesi T, Cusulin JIW, Koblinger K, Whelan PJ, Pittman QJ & Bains JS (2013). Noradrenaline is a stress-associated metaplastic signal at GABA synapses. *Nat Neurosci* **16**, 605–612.

- Itoi K, Talukder AH, Fuse T, Kaneko T, Ozawa R, Sato T, Sugaya T, Uchida K, Yamazaki M, Abe M, Natsume R & Sakimura K (2014). Visualization of corticotropin-releasing factor neurons by fluorescent proteins in the mouse brain and characterization of labeled neurons in the paraventricular nucleus of the hypothalamus. *Endocrinology* **155**, 4054–4060.
- Joëls M & Baram TZ (2009). The neuro-symphony of stress. *Nat Rev Neurosci* **10**, 459–466.
- Kim JS, Han SY & Iremonger KJ (2019). Stress experience and hormone feedback tune distinct components of hypothalamic CRH neuron activity. *Nat Commun* **10**, 1–15.
- Kim K-S & Han P-L (2006). Optimization of chronic stress paradigms using anxiety- and depression-like behavioral parameters. *J Neurosci Res* **83**, 497–507.
- Kirschbaum C, Prüssner JC, Stone AA, Federenko I, Gaab J, Lintz D, Schommer N & Hellhammer DH (1995). Persistent high cortisol responses to repeated psychological stress in a subpopulation of healthy men. *Psychosom Med* **57**, 468–474.
- Kiss A & Aguilera G (1993). Regulation of the hypothalamic pituitary adrenal axis during chronic stress: responses to repeated intraperitoneal hypertonic saline injection. *Brain Res* **630**, 262–270.
- Korosi A, Shanabrough M, McClelland S, Liu Z-W, Borok E, Gao X-B, Horvath TL & Baram TZ (2010). Early-life experience reduces excitation to stress-responsive hypothalamic neurons and reprograms the expression of corticotropin-releasing hormone. *J Neurosci Off J Soc Neurosci* **30**, 703–713.
- Kourrich S, Calu DJ & Bonci A (2015). Intrinsic plasticity: an emerging player in addiction. *Nat Rev Neurosci* **16**, 173–184.
- Kourrich S & Thomas MJ (2009). Similar Neurons, Opposite Adaptations: Psychostimulant Experience Differentially Alters Firing Properties in Accumbens Core versus Shell. *J Neurosci* **29**, 12275–12283.
- Kovács KJ (1998). Invited review c-Fos as a transcription factor: a stressful (re)view from a functional map. *Neurochem Int* **33**, 287–297.
- Kudielka BM, von Känel R, Preckel D, Zraggen L, Mischler K & Fischer JE (2006). Exhaustion is associated with reduced habituation of free cortisol responses to repeated acute psychosocial stress. *Biol Psychol* **72**, 147–153.
- Kusek M, Tokarski K & Hess G (2013). Repeated restraint stress enhances glutamatergic transmission in the paraventricular nucleus of the rat hypothalamus. *J Physiol Pharmacol Off J Pol Physiol Soc* **64**, 565–570.
- Kuzmiski JB, Marty V, Baimoukhametova DV & Bains JS (2010). Stress-induced priming of glutamate synapses unmasks associative short-term plasticity. *Nat Neurosci* **13**, 1257–1264.
- Lisman J, Cooper K, Sehgal M & Silva AJ (2018). Memory formation depends on both synapse-specific modifications of synaptic strength and cell-specific increases in excitability. *Nat Neurosci* **21**, 309–314.
- Luther JA, Daftary SS, Boudaba C, Gould GC, Halmos KC & Tasker JG (2002). Neurosecretory and non-neurosecretory parvocellular neurones of the hypothalamic paraventricular nucleus express distinct electrophysiological properties. *J Neuroendocrinol* **14**, 929–932.
- Ma XM, Lightman SL & Aguilera G (1999). Vasopressin and corticotropin-releasing hormone gene responses to novel stress in rats adapted to repeated restraint. *Endocrinology* **140**, 3623–3632.
- Marzban F, Tweedle CD & Hatton GI (1992). Reevaluation of the plasticity in the rat supraoptic nucleus after chronic dehydration using immunogold for oxytocin and vasopressin at the ultrastructural level. *Brain Res Bull* **28**, 757–766.
- McEwen BS & Seeman T (1999). Protective and damaging effects of mediators of stress. Elaborating and testing the concepts of allostasis and allostatic load. *Ann N Y Acad Sci* **896**, 30–47.
- Melia KR, Ryabinin AE, Schroeder R, Bloom FE & Wilson MC (1994). Induction and habituation of immediate early gene expression in rat brain by acute and repeated restraint stress. *J Neurosci Off J Soc Neurosci* **14**, 5929–5938.
- Miklós IH & Kovács KJ (2012). Reorganization of synaptic inputs to the hypothalamic paraventricular nucleus during chronic psychogenic stress in rats. *Biol Psychiatry* **71**, 301–308.
- Miyata S, Nakashima T & Kiyohara T (1994). Structural dynamics of neural plasticity in the supraoptic nucleus of the rat hypothalamus during dehydration and rehydration. *Brain Res Bull* **34**, 169–175.
- O'Leary T, Williams AH, Franci A & Marder E (2014). Cell Types, Network Homeostasis, and Pathological Compensation from a Biologically Plausible Ion Channel Expression Model. *Neuron* **82**, 809–821.
- Ons S, Rotllant D, Marín-Blasco IJ & Armario A (2010). Immediate-early gene response to repeated immobilization: Fos protein and arc mRNA levels appear to be less sensitive than c-fos mRNA to adaptation. *Eur J Neurosci* **31**, 2043–2052.
- Pangrčić T, Potokar M, Haydon PG, Zorec R & Kreft M (2006). Astrocyte swelling leads to membrane unfolding, not membrane insertion. *J Neurochem* **99**, 514–523.
- Rho JH & Swanson LW (1989). A morphometric analysis of functionally defined subpopulations of neurons in the paraventricular nucleus of the rat with observations on the effects of colchicine. *J Neurosci Off J Soc Neurosci* **9**, 1375–1388.
- Salter E, Sunstrum J, Matovic S & Inoue W (2018). Chronic stress dampens excitatory synaptic gain in the paraventricular nucleus of the hypothalamus. *J Physiol*; <https://doi.org/10.1113/JP275669>.
- Schulz DJ (2006). Plasticity and stability in neuronal output via changes in intrinsic excitability: it's what's inside that counts. *J Exp Biol* **209**, 4821–4827.
- Sensel L, Baimoukhametova D, Sterley T-L & Bains JS (2016). Sexually dimorphic neuronal responses to social isolation. *eLife* **5**, e18726.
- Stamp JA & Herbert J (1999). Multiple immediate-early gene expression during physiological and endocrine adaptation to repeated stress. *Neuroscience* **94**, 1313–1322.
- Sterley T-L, Baimoukhametova D, Füzesi T, Zurek AA, Daviu N, Rasiah NP, Rosenecker D & Bains JS (2018). Social transmission and buffering of synaptic changes after stress. *Nat Neurosci* **21**, 393–403.

- Tasker JG & Dudek FE (1991). Electrophysiological properties of neurones in the region of the paraventricular nucleus in slices of rat hypothalamus. *J Physiol* **434**, 271–293.
- Taylor AL (2012). What we talk about when we talk about capacitance measured with the voltage-clamp step method. *J Comput Neurosci* **32**, 167–175.
- Theodosis DT & Poulain DA (1984). Evidence for structural plasticity in the supraoptic nucleus of the rat hypothalamus in relation to gestation and lactation. *Neuroscience* **11**, 183–193.
- Tremblay M-È, Lowery RL & Majewska AK (2010). Microglial interactions with synapses are modulated by visual experience. *PLoS Biol* **8**, e1000527.
- Uchida S, Nishida A, Hara K, Kamemoto T, Suetsugi M, Fujimoto M, Watanuki T, Wakabayashi Y, Otsuki K, McEwen BS & Watanabe Y (2008). Characterization of the vulnerability to repeated stress in Fischer 344 rats: possible involvement of microRNA-mediated down-regulation of the glucocorticoid receptor. *Eur J Neurosci* **27**, 2250–2261.
- Ulrich-Lai YM & Herman JP (2009). Neural regulation of endocrine and autonomic stress responses. *Nat Rev Neurosci* **10**, 397–409.
- Verkuyl JM, Hemby SE & Joëls M (2004). Chronic stress attenuates GABAergic inhibition and alters gene expression of parvocellular neurons in rat hypothalamus. *Eur J Neurosci* **20**, 1665–1673.
- Wamsteeker Cusulin JI, Füzesi T, Inoue W & Bains JS (2013a). Glucocorticoid feedback uncovers retrograde opioid signaling at hypothalamic synapses. *Nat Neurosci* **16**, 596–604.
- Wamsteeker Cusulin JI, Füzesi T, Watts AG & Bains JS (2013b). Characterization of corticotropin-releasing hormone neurons in the paraventricular nucleus of the hypothalamus of Crh-IRES-Cre mutant mice. *PLoS One* **8**, e64943.
- Wang LA, Nguyen DH & Mifflin SW (2019). Corticotropin-releasing hormone projections from the paraventricular nucleus of the hypothalamus to the nucleus of the solitary tract increase blood pressure. *J Neurophysiol* **121**, 602–608.
- Yuan Y, Wu W, Chen M, Cai F, Fan C, Shen W, Sun W & Hu J (2019). Reward Inhibits Paraventricular CRH Neurons to Relieve Stress. *Curr Biol CB* **29**, 1243–1251.e4.
- Zdilla MJ, Hatfield SA, McLean KA, Cyrus LM, Laslo JM & Lambert HW (2016). Circularity, Solidity, Axes of a Best Fit Ellipse, Aspect Ratio, and Roundness of the Foramen Ovale: A Morphometric Analysis With Neurosurgical Considerations. *J Craniofac Surg* **27**, 222–228.
- Zhang W & Linden DJ (2003). The other side of the engram: experience-driven changes in neuronal intrinsic excitability. *Nat Rev Neurosci* **4**, 885–900.
- Zhang X-F, Hu X-T & White FJ (1998). Whole-Cell Plasticity in Cocaine Withdrawal: Reduced Sodium Currents in Nucleus Accumbens Neurons. *J Neurosci* **18**, 488–498.
- Zhang Z & Bourque CW (2003). Osmometry in osmosensory neurons. *Nat Neurosci* **6**, 1021–1022.

Additional information

Competing interests

None.

Author contributions

SM designed the experiments, acquired, analysed and interpreted the data, and drafted the article. AI, HI, XFW, JS and EWS acquired, analysed and interpreted the data. ESK and JMT developed custom MATLAB and analysed the data electrophysiologically. MH, NV, MET acquired, analysed and interpreted the electron microscopy data. WI conceived and designed the experiments and drafted the article.

Funding

Canadian Institute for Health Research: Wataru Inoue PJT 148707; Natural Sciences and Engineering Research Council of Canada: Wataru Inoue 06106-2015 RGPIN; Mental Health Foundation Canada: Wataru Inoue NA.

Acknowledgements

We thank all members of Inoue lab for thoughtful inputs to the project. We are grateful to Ms Irma Meteluch for her help with animal husbandry. We also thank Dr Jaideep Bains (University of Calgary) for his constructive comments on early versions of the manuscript.

Keywords

intrinsic excitability, neuroendocrine, paraventricular nucleus of the hypothalamus, plasticity, stress

Supporting information

Additional supporting information may be found online in the Supporting Information section at the end of the article.

Statistical Summary Document